Journal of Power Sources 254 (2014) 268–276

Contents lists available at ScienceDirect

Journal of Power Sources

journal homepage: www.elsevier.com/locate/jpowsour

Low-temperature charging of lithium-ion cells Part II: Model reduction and application

Jürgen Remmlinger [a,*], Simon Tippmann [b], Michael Buchholz [a], Klaus Dietmayer [a]

[a] Institute of Measurement, Control, and Microtechnology, Ulm University, Albert-Einstein-Allee 41, D-89081 Ulm, Germany
[b] Deutsche ACCUmotive GmbH & Co. KG, Neue Str. 95, D-73230 Kirchheim/Teck, Germany

HIGHLIGHTS

- Model reduction of an electrochemical model.
- New identification-based model reduction process.
- On-board applicable, linear parameter-varying model as a result of model reduction.
- Application of the reduced model in charging control.
- Reduction of charging duration for low-temperature charging of lithium-ion cells.

ARTICLE INFO

Article history:
Received 16 October 2013
Received in revised form
29 November 2013
Accepted 19 December 2013
Available online 30 December 2013

Keywords:
Li-ion cell
Lithium-plating
Model-reduction
LPV model
Charging control

ABSTRACT

Lithium-ion cells, especially when used in electric vehicles at varying operation conditions, require a sophisticated battery management to ensure an optimal operation regarding operation limits, performance, and maximum lifetime. In some cases, the best trade-off between these conflictive goals can only be reached by considering internal, non-measurable cell characteristics. This article presents a data-driven model-reduction method for a strict electrochemical model. The model describes the charging process of a lithium-ion cell and possibly occurring degradation effects in a large temperature range and is presented in Part I of this contribution. The model-reduction process is explained in detail, and the gained model is compared to the original electrochemical model showing a very high approximation quality. This reduced model offers a very low computation complexity and is therefore suitable for the implementation in a battery management system (BMS). Based on this model, an advanced charging strategy is presented and evaluated for possible reductions in charging times especially at low temperatures.

1. Introduction

Lithium-ion batteries are a key component in current and prospective electric vehicles. For an appropriate operation of these batteries which has to ensure high performance and long lifetime, monitoring of the cells is essential. On the one hand, the available power and the resulting possible driving range in the present operation point have to be determined. On the other hand, the state-of-health (SOH) of the cells has to be identified since aging (i.e. degradation of the battery) can occur due to different reasons. To recognize degradation, usually the effects of aging, i.e. a loss of capacity or a rise of the internal resistance, are monitored [1].

As cell degradation is strongly depending on the operation conditions, an operation strategy preventing or reducing degradation is necessary beyond cell monitoring. In simple cases, this can be reached through operation limits usually depending on measurable signals, e.g. current or temperature of the cells. However, extended operation strategies require a more accurate understanding and description of the degradation mechanisms.

One method of gaining this knowledge on degradation is strict electrochemical modeling, which allows a deeper insight in non-measurable cell characteristics, e.g. anode potential as indicator for metallic lithium deposition (lithium plating) during charging. Such an electrochemical model describing the charging process of lithium-ion cells at low temperatures is worked out in Part I [2] of this contribution. In detail, a 1D + 1D (pseudo-2D) model based on [3,4] calculating the lithium-ion concentration in surface and particle radius direction is set up over a wide temperature (−25 °C to

* Corresponding author. Tel.: +49 731 50 26308.
E-mail address: juergen.remmlinger@uni-ulm.de (J. Remmlinger).

0378-7753/$ – see front matter © 2014 Elsevier B.V. All rights reserved.
http://dx.doi.org/10.1016/j.jpowsour.2013.12.101

40 °C) and current range (0.1 C–6 C). This temperature and current range even exceeds the operation range relevant for the assessment of charging at low-temperatures. Additionally, the complex model is parameterized and validated with cell measurements and analyzed regarding the ability to predict harming cell states.

Advanced operation management or diagnosis methods based on such electrochemical models allow to use additional, non-measurable information from within the model, but require that these models are calculated online. Hence, for the application within a model-based on-board control avoiding adverse system states, a reduction of the complex model is necessary to fulfill the challenging computational and real-time requirements of the battery management system (BMS). These are, in detail, a low complexity model with focus on good approximation of the original electrochemical model for the selected signals, a realization in a discrete-time not requiring a solver, and, as a result, a low execution time.

A model reduction can be performed e.g. through approximations and mathematical simplifications. In these model reduction steps, the original electrochemical character of the model is retained and only the level of abstraction is enlarged. This leads to a reduction of the model complexity, but not necessarily to a reduction of the computational load.

In this contribution, model-reduction based on system identification methods is introduced, resulting in models for terminal voltage and anode potential prediction. These models are identified from input and output signal data sets retrieved from the original electrochemical model. Thus, the reduction of the model is done implicitly by approximating the input/output behavior. To yield a good approximation, the input signals for the generation of data sets by simulation have to show a high excitation and cover the whole state-of-charge (SOC) and temperature range of the validated electrochemical model. Using this simulation data, each model is identified fulfilling the given on-board requirements. A discrete-time linear parameter-varying (LPV) model is chosen as model form, because these models are known to reproduce well the complex nonlinear behavior of lithium-ion battery cells and still fulfill these requirements [5].

With the reduced anode potential model, it is possible to simulate the anode potential at the anode-separator interface. In Ref. [2], this potential is shown to give the best indicator for a degradation during charging. Therefore, as an additional contribution of this paper, this model is used to develop an advanced charging control preventing degradation and still delivering maximum performance at every operation point.

The paper is organized as follows: The proposed model reduction method is presented in detail in Section 2. The reduced models are assessed and compared to the original electrochemical model in Section 3. The application of the gained anode potential model within an advanced charging strategy is discussed in Section 4. The contribution closes with conclusions and an outlook on further work in Section 5.

2. Model reduction

In literature, reduction of electrochemical models yielding an on-board applicable model with low complexity is commonly done by mathematical simplifications based on approximations and a higher abstraction level, see e.g. Refs. [6–9]. The resulting reduced models are still physically motivated. However, the equivalence of the original and the reduced model for one parameter set is not guaranteed for a given cell, and in some cases parameters of the reduced model have to be fitted due to the approximations, resulting in a limited physical meaning. Additionally, these models are still continuous-time descriptions and therefore require solver functions, which is a serious drawback for on-board implementations. If it is possible to transform such a reduced model to an equivalent discrete-time formulation with fixed sample time, the physical meaning of the parameters gets lost.

In contrast to this classical approach which retains the basic physical-electrochemical structure of the model, the proposed method focuses on the discrete-time approximation of the input/output behavior of the original model, whereas the structure of the underlying model is arbitrary, as long as it fulfills the requirements of on-board applicability. This model reduction approach is based on the idea of black-box system identification [10], where the discrete-time input/output behavior of a dynamical system with unknown internal structure and parameters (a “black box” we have no insight into) is estimated from measurement data sets of the input and output signals. Instead of measurements of inputs and outputs of a system, simulated data from the original electrochemical model is used in this work to build the data sets required for the identification process, which in this case yields the reduced and discrete-time model description with a structure independent of the original model’s internal structure. The choice of model structure leaves more degrees of freedom to fit the input/output behavior well even with very simple models. In Refs. [11,12], a related identification-based approach was used to retrieve a reduced electrical model of a solid oxide fuel cell (SOFC).

The specific electrochemical model used in this work is described in Part I [2] and was implemented in COMSOL. The common interface of the original electrochemical model and each of the two application-oriented reduced models are the input and output signals. These signals are the applied current I, the initial SOC, and the cell temperature T as inputs as well as the terminal voltage U or the potential vs. Li/Li^+ at the anode-separator interface ϕ as outputs, respectively. The latter is chosen from the numerous signals available in the space-resolved electrochemical model as it is most suitable and also sufficient to indicate degradation during charging processes due to metallic lithium deposition. For charging processes, this point of the anode will always be the one with the lowest potential as described in Part I of this contribution [2].

In Subsection 2.1, the basic structure of the reduced cell models is introduced, where the output signals are assumed to be the superposition of a static and a dynamic model part. A detailed description of the identification data is given in Subection 2.2. Subspace identification, which is one possible method for black-box system identification, is introduced and utilized in Subection 2.3 to identify the dynamic parts of the reduced models from the identification data sets. As this identification is done separately for

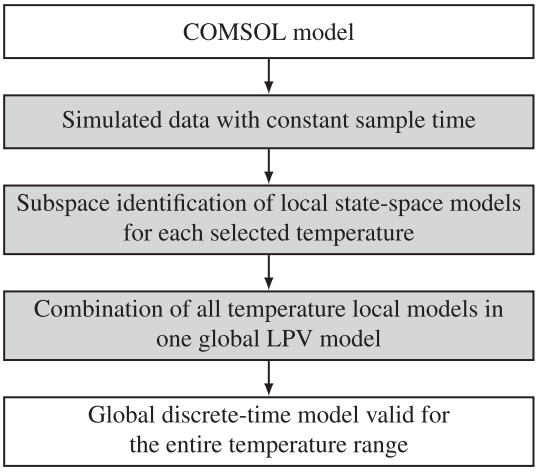

Fig. 1. Overall schedule of the model reduction process using system identification.

several isothermal data sets, i.e. for several, but constant cell temperatures, Subection 2.4 describes how to combine these temperature local models into one global LPV model valid for the entire temperature range. The complete model reduction process is summarized in Fig. 1.

2.1. Cell model

In application-oriented modeling of the electrical input/output behavior of lithium-ion cells, equivalent circuits (EC) are a common basis. For such EC models, a separation is made into a static model part describing the open circuit voltage (OCV) of the battery cell and a dynamic model part describing the overvoltage in an EC, like depicted in Fig. 2 (cf. e.g. Refs. [13,14]). This approach is motivated by the fact that in steady state, the terminal voltage, which is the sum of cathode and anode half-cell potentials, depends statically on several input and cell parameters. During or shortly after dynamic operation, deviations from this steady state occur due to dynamic processes in the cell. These processes vanish if steady state is reached again. The anode potential describes one of the two half-cell potentials the terminal voltage is composed of. Therefore, this approach is transferred to the structure of the anode potential model, as illustrated in Fig. 2.

Like usual, the static parts are modeled as static nonlinear relations between SOC and OCV in this work. However, the EC model usually used for the dynamic part is replaced by identified discrete-time LPV models in state-space form (see Subections 2.3 and 2.4). The LPV models are able to represent nonlinear effects of temperature and SOC on the dynamic overvoltages and the dynamic deviations from the static anode potential values, respectively. For the identification of the dynamic model parts, the SOC dependent static open-circuit voltage and static anode potential are subtracted from the absolute terminal voltage and absolute anode potential, respectively. In the overall models, these values from the static relations are again added to the outputs of the respective identified dynamic models according to Fig. 2.

2.2. Identification data

To collect the data sets for identification of the reduced models, the original electrochemical model [2] is simulated isothermally using its COMSOL implementation. Isothermal simulations offer the advantage of a separate, decoupled identification of the electrical cell characteristics without disturbances by thermal influences on the input/output behavior. This is done for several cell temperature values separately to identify the parameters with respect to cell temperature. This allows to couple a thermal model after the identification process. Such a thermal model is not only cell dependent (e.g. self-heating), but also has to incorporate the battery packaging (e.g. thermal coupling of cells or cooling) and is not within the scope of this work.

To guarantee that the simulated data sets represent all original model properties, it is necessary to simulate the model within the whole operation range and with sufficient excitation. Therefore, current pulse profiles as given in Fig. 3 were used as input signals for the simulations. These alternating current pulse profiles show a 10 min charge duration followed by a 10 min rest duration. The current amplitude of these pulses is constant for one simulation run except for higher SOC values, where the current is controlled to ensure a voltage below the charging voltage limit. For different simulation runs, the current amplitudes varies in the range of 0.1 C–1 C. The isothermal simulations are carried out for cell temperatures in the range of −20 °C–40 °C, which is the complete range the original electrochemical model was designed and validated for, with a constant difference of 5 K, each starting from 0% SOC. The step size of 5 K was chosen to guarantee good interpolation results for the whole temperature range. If a reduction of simulation time of the COMSOL model is desired, the temperature step size could be increased with raising temperature, because the nonlinear temperature influence is significantly higher at lower temperatures.

Although a much smaller sample time is used in the COMSOL simulation, signals are recorded with a constant sample time of 1 s for identification purposes, because the sample time of the data sets also determines the sample time of the identified models. Within an application for charging scenarios, this sample time is a good compromise regarding the number of required model evaluations, i.e. the computational load, and covering of current dynamics.

The COMSOL simulation was controlled by LiveLink for MATLAB to run the different simulation scenarios successively. Even though simulations in COMSOL are not always possible without manual user interactions, consistent data sets could be generated with this procedure which are the basis in the following model identification process.

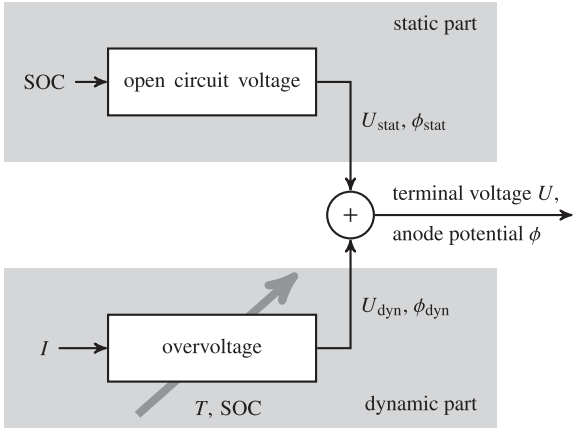

Fig. 2. Structure of the application-oriented reduced cell models for terminal voltage and anode potential.

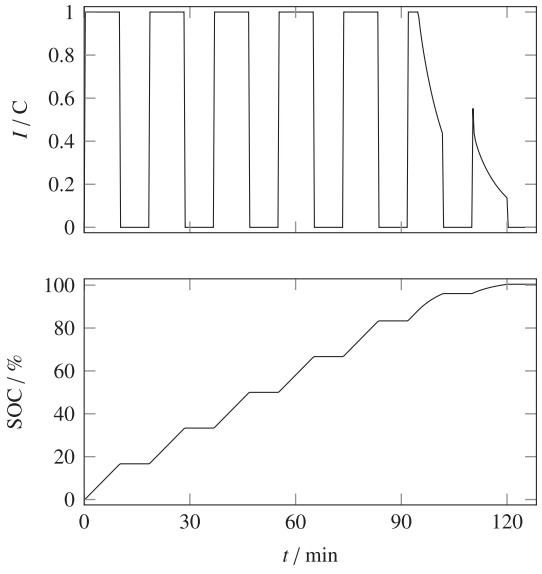

Fig. 3. Current profile for identification data sets.

2.3. Subspace identification

For the identification of the temperature local models, subspace identification is used. Subspace identification (SID), or subspace-based state-space system identification (4SID) at length, denotes a class of black-box identification methods that estimate non-iteratively the order as well as the parameters of a dynamic system. Classical algorithms in this class of identification methods are "Canonical Variate Analysis" (CVA, cf. Refs. [15,16]), "Numerical Algorithms for Subspace-based State-Space System Identification" (N4SID, cf. Refs. [17,18]), "Multivariable Output Error State Space Identification" (MOESP, cf. [19,20]), and "Predictor-Based Subspace-Identification" (PBSID,[1], cf. Refs. [21,22]). In their basic versions, they all result in a discrete-time state-space description of a linear and time-invariant (LTI) system

$$\boldsymbol{x}(k+1) = \boldsymbol{A}\boldsymbol{x}(k) + \boldsymbol{B}\boldsymbol{u}(k), \tag{1a}$$

$$\boldsymbol{y}(k) = \boldsymbol{C}\boldsymbol{x}(k) + \boldsymbol{D}\boldsymbol{u}(k), \tag{1b}$$

where $\boldsymbol{u} \in \mathbb{R}^{n_u}$ and $\boldsymbol{y} \in \mathbb{R}^{n_y}$ denote the inputs and outputs, respectively. The state vector $\boldsymbol{x} \in \mathbb{R}^n$ as well as the system parameter matrices $\boldsymbol{A}$, $\boldsymbol{B}$, $\boldsymbol{C}$, and $\boldsymbol{D}$ are not known in advance of the identification process, and the order n of the system is also unknown. A recent and detailed overview on these subspace methods is given in Ref. [23], older surveys like Refs. [24–26] do not comprise the relatively young PBSID methods. In this work, an implementation similar to [27] of the PBSID is used to identify one LTI model for each simulated cell temperature and output signal.

As described before, the dynamic parts of the models for terminal voltage and anode potential depend nonlinearly on temperature and SOC. Since only data of one single temperature is used for each LTI model, a temperature influence has not to be taken into account for identification of these models. Nevertheless, SOC is still varying in the whole range from 0% to 100%. However, the applied PBSID method works only for LTI systems. To resolve this issue, a bilinear approach for the models' input is used. In this approach, an extended model input is formed based on an SOC dependent B-spline and the cell current. With B-splines [28], a nonlinear curve $S(l)$ can be represented by a linear combination of weighted basis B-splines $s_{i,v}$, where every $s_{i,v}$ is a piecewise defined function of degree v and unequal to 0 only for a limited subrange of the independent variable l, see Ref. [28] for a definition. The basis B-splines of degree v are thereby weighted with $w - v - 1$ so-called control points p_i:

$$S(l) = \sum_{i=0}^{w-v-2} p_i s_{i,v}(l), \tag{2}$$

$$= \boldsymbol{p}^{\mathrm{T}} \boldsymbol{s}_v(l). \tag{3}$$

In the state-space-model (1) for the specific configuration of the battery cell model in this work, where we have the current I as a single input and terminal voltage or anode potential as the only output, the parameter matrices $\boldsymbol{B}$ and $\boldsymbol{D}$ are only a vector $\boldsymbol{b}$ and a scalar d, respectively. The elements of $\boldsymbol{b}$ as well as d are depending on the SOC in an unknown and nonlinear manner. B-splines can be used to transfer the nonlinear problem to a linear problem, as shown for $\boldsymbol{b}(\mathrm{SOC})$:

$$\boldsymbol{b}(\mathrm{SOC})u = \boldsymbol{S}(\mathrm{SOC})u \tag{4}$$

$$= \left(\boldsymbol{P}^{\mathrm{T}} \boldsymbol{s}_v(\mathrm{SOC})\right) u \tag{5}$$

$$= \underbrace{\boldsymbol{P}^{\mathrm{T}}}_{\boldsymbol{B}_{\mathrm{ext}}} \underbrace{\boldsymbol{s}_v(\mathrm{SOC})\, u}_{\boldsymbol{u}_{\mathrm{ext}}} \tag{6}$$

where u equals the original input current I, $\boldsymbol{S}(\mathrm{SOC})$ is a vector of B-splines with the same basis B-splines $\boldsymbol{s}_v$, and $\boldsymbol{P}^{\mathrm{T}}$ is the matrix containing the control points row-wise for each element of the original vector $\boldsymbol{b}(\mathrm{SOC})$. This a-priori unknown matrix of control points can now be identified as the new linear input matrix $\boldsymbol{B}_{\mathrm{ext}}$, if the new extended input $\boldsymbol{u}_{\mathrm{ext}}$ built from the a-priori known, SOC dependent basis B-splines and the current is within the SID algorithm. The same approach can analogously be used for $d(\mathrm{SOC})$, resulting in the same extended input $\boldsymbol{u}_{\mathrm{ext}}$ if the same basis B-splines are used, and a generalization for systems with multiple outputs is straightforward. For multiple inputs, the solution can be retrieved element-wise for each input i and appropriate stacking of the resulting matrices $\boldsymbol{B}_{i,\mathrm{ext}}$ and extended inputs $\boldsymbol{u}_{i,\mathrm{ext}}$.

Here, B-splines of degree 2 with 6 control points clamped in the range of 0%–100% SOC are used to approximate the nonlinear dependence of the model parameters on different SOC values. Accordingly, the extended input vector at sample time k is given by

$$\boldsymbol{u}_{\mathrm{ext}}(k) = \begin{bmatrix} s_0(\mathrm{SOC}(k))I(k) \\ s_1(\mathrm{SOC}(k))I(k) \\ \vdots \\ s_5(\mathrm{SOC}(k))I(k) \end{bmatrix}. \tag{7}$$

In a similar way, nonlinearities in current amplitude, especially occurring at low temperatures, can be handled. To cover this influence, an extension of the original input with Laguerre polynomials (see e.g. Ref. [29]) is used. Thereby, an approximation with third-order Laguerre polynomials of the nonlinearities depending on current amplitude proved to be sufficient. To combine both extensions, a Kronecker product (see e.g. Ref. [30] for a definition) between the basis B-splines $\boldsymbol{s}_v(\mathrm{SOC})$ and the Laguerre basis functions is used, resulting in a further increased number of 18 inputs in the extended input vector and an appropriately dimensioned input matrix $\boldsymbol{B}_{\mathrm{ext}}$. With these modifications, the SID is carried out for all single temperatures and each of the two output signals terminal voltage and anode potential, resulting in LTI models each with 18 inputs (7) and one output. During the identification process, a model order of three was determined for both output signals. A validation of the single temperature models can be found in Section 3.1.

2.4. Global model

After the model identification step, several models, each valid for one specific cell temperature, exist for both outputs. Due to the fact that the identification data can be retrieved easily from simulation, it can be assumed that the sampling distance of temperature is chosen close enough so that a linear interpolation between two neighboring models is valid for temperature values in between. To allow for an easy simulation of the model with continuously varying cell temperatures within the whole operating range, a global model is necessary.

Here, a linear parameter-varying (LPV) model is considered as the global model form. For a discrete-time state-space description, the LPV model has the following form:

$$\boldsymbol{x}(k+1) = \sum_{i=1}^{m} \mu_i(k)(\boldsymbol{A}_i\boldsymbol{x}(k) + \boldsymbol{B}_i\boldsymbol{u}(k)) \tag{8}$$

[1] In this paper, PBSID always refers to the optimized version of the predictor-based SID that is also called PBSIDopt in some publications.

$$\boldsymbol{y}(k) = \sum_{i=1}^{m} \mu_i(k)(\boldsymbol{C}_i\boldsymbol{x}(k) + \boldsymbol{D}_i\boldsymbol{u}(k)). \tag{9}$$

The LPV model can be seen as a weighted sum of local LTI models, where the weighting, the so-called scheduling signals $\mu_i(k)$, are time-varying. In other words, LPV models are able to reproduce the nonlinear behavior of a system by changing their behavior according to the scheduling signals, but still retain a linear characteristic if the scheduling signal remains constant.

To describe the linear interpolation of the temperature local LTI models within the LPV framework, the scheduling signals μ_i are a function of temperature and are defined as

$$\boldsymbol{\mu}_i(k) = \begin{cases} 1 - \frac{T_i - T(k)}{T_i - T_{i-1}}, & \text{if } T_{i-1} \le T(k) \le T_i, \\ 1 - \frac{T(k) - T_i}{T_{i+1} - T_i}, & \text{if } T_i \le T(k) \le T_{i+1}, \\ 0, & \text{otherwise}, \end{cases} \tag{10}$$

where T_i denotes the valid temperature for the i-th LTI model and the models are numbered with increasing temperature. To yield a valid interpolation of the local LTI models, it is necessary that their states $\boldsymbol{x}$ are all described using identical basis vectors for the state space. In the case of subspace identification, the state-space basis is unknown. Therefore, the local LTI models have to be transformed into one common state-space description. Here, a transformation of the LTI models into their observable canonical form (see e.g. Ref. [31]) is used. This choice additionally reduces the number of parameters which have to be interpolated to a minimum, because the observable canonical form is a state-space realization of a system with the minimum number of free parameters.

With this LPV model approach, the two global models, one for terminal voltage and one for anode potential, are built from the temperature local LTI state-space models. Including these models as the dynamic part in the respective overall cell models (cf. Subection 2.1 and Fig. 2), one yields the final reduced cell models for terminal cell voltage and anode potential.

3. Assessment of the reduced models

The reduced models can now be used to substitute the original electrochemical model for charging scenarios in the operation range used for identification. To prove this, the reduced models are validated against the original model in Subection 3.1. Afterward, the advantages of the reduced models are shown in Subection 3.2.

3.1. Model validation

For model validation, beside a qualitative check for a reasonable model behavior, a quantitative measure of the model fit is necessary. Here, the evaluation of the model quality is done by two measures. The first one is the so-called Variance Accounted For (VAF) [32], a measure for the dynamic fit of the model. The VAF value is calculated from the model error $e = y_{\text{ref}} - y_{\text{model}}$ and is always in the range of 0%–100%, where higher values indicate a better model fit:

$$\text{VAF} = \max\left\{1 - \frac{\text{var}(e)}{\text{var}\left(y_{\text{ref}}\right)}, 0\right\} \times 100\%. \tag{11}$$

The second measure used here is the mean absolute error (MAE). The MAE is a mean of the absolute model errors for all measurement time points

$$\text{MAE} = \frac{1}{N}\sum_{i=1}^{N} |e_i|. \tag{12}$$

This measure is an indicator for the static fit of the model behavior.

At first, a validation using the identification data sets is carried out. The reference signal for evaluation is either the terminal voltage or the anode potential simulated with the electrochemical model. The model value is the corresponding signal simulated with the reduced model. As these identification data sets are gained by isothermal simulation runs, the reduced model is only validated at the temperature sampling points, i.e. only the respective single LTI model is active. Thereby, a maximum MAE of 0.0119 V for terminal voltage and of 0.0073 V for anode potential was observed. The VAF value is always higher than 99.35% for terminal voltage and 99.0% for anode potential. These maximum errors are observed for the identification data sets with the lowest temperature and are decreasing for higher temperature values. For the whole operating rang, the gained low complexity models give very good approximations of the outputs of the original electrochemical model for the identification data sets.

The same evaluation procedure is also performed for validation data sets not included in the model identification process. Hereby, the original electrochemical model is simulated with a current profile as described in Section 2.2 with the difference that current values and duration of pulses and resting times are varied randomly. This current profile is shown in Fig. 4 together with the simulation results for terminal voltage and anode potential. It can be seen that outputs from the reduced models (blue) match the reference signals (orange) very well with respect to static offset as well as dynamic behavior. Even in the magnified view for anode potential in Fig. 4, almost no deviation is observable.

All investigations so far have been for validation of the single temperature models and the respective parts of the static nonlinear characteristic. A further validation with varying cell temperature is shown in Fig. 5. Here, additionally to the randomly altering current, the cell temperature (green) in the COMSOL simulation rises with a constant slope. Temperature varies in this validation example from 10 °C to almost 30 °C. The influence of the temperature on the dynamic behavior of terminal voltage and anode potential is

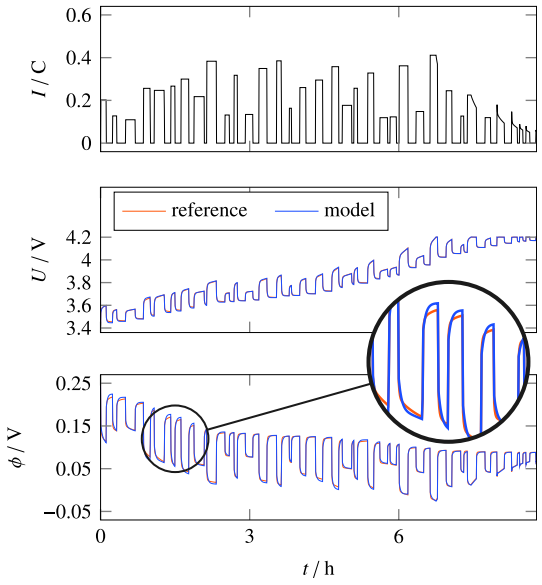

Fig. 4. Validation for isothermal data at cell temperature 0 °C.

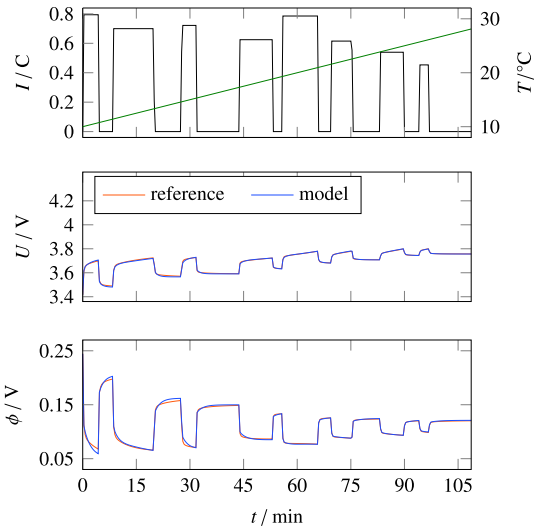

Fig. 5. Validation for linear increasing cell temperature starting at 10 °C.

evident from this figure. Even for this more complex scenario, where the linear interpolation of the dynamic model part is active, a good match of reduced model and reference is achieved. For both data sets, it is also observable that the static as well as the dynamic model parts in the reduced models describe the behavior correct. Whereas the dynamic model part only influences the behavior during and shortly after current changes, the static model represents the steady state behavior, i.e. the behavior in the end of the resting periods following the current pulses. Model errors for the two described validation data sets are quantitatively summarized in Tab. 1.

3.2. Analysis of the reduced models

One aim motivating the model reduction was the decrease of computational load. To give an idea of the differences in simulation time for the original COMSOL model and the reduced models implemented in Simulink, a comparison for the two described validation data sets is given in Tab. 2. All simulations are done on a common desktop computer. Although such a configuration is not useful to judge absolute calculation times with respect to an on-board implementation, it can show the relative difference between the two model forms. For the isothermal validation run with an overall real-time duration of more than 8.5 h, the COMSOL simulation lasts approximately 42 min and the Simulink simulation of the reduced models less than 8 s. For the shorter temperature varying validation data set, a comparable duration ratio can be observed with a possibly slightly higher computational overhead for shorter data sets in the Simulink simulation. In these examples, the Simulink simulation needs 1/325 to 1/250 of the simulation time of the COMSOL model for the same simulation input, and still delivers very good results for the outputs of the models as shown above.

Thereby, the shorter simulation time is gained by several limitations in the reduced model. The reduced model is only valid for the charging scenarios regarded in this paper. The electrochemical model will possibly be applicable in a more general way. Furthermore, the reduced model can only be evaluated for the constant sample time of the model, which is rather an advantage, especially for on-board application.

Table 1
Validation error.

Profile	VAF (U)	MAE (U)	VAF (φ)	MAE (φ)
$T = 0$ °C, isothermal	99.65%	0.0029 V	99.49%	0.0023 V
varying T	99.73%	0.0027 V	99.71%	0.0015 V

Table 2
Comparison of simulation time.

Real time	Simulation time COMSOL	Simulation time Simulink
526.5 min	42.1 min	7.751 s
108.7 min	8.4 min	2.049 s

One possible application for both the electrochemical and consequently the reduced models is the calculation of a so-called degradation map already introduced in Part I [2] of this contribution. A degradation map based on the degradation factor $\Theta_{\phi}^{\text{nom}}$, which contains the ratio of the load charged under harming conditions ($\varphi < 0$) and the overall charged load for a full load cycle, is regarded exemplarily in the following. For a given charging current and temperature, the value of the map corresponds to the degradation effect. The degradation map given in Fig. 6 is calculated with the reduced model in a much shorter time even for a finer temperature and current grid. Thereby, in comparison to the map calculated with the electrochemical model (Fig. 12 in Part I [2]), almost no deviation is present.

To determine a non-harming and consequently allowed current for fully charging the battery cell, the degradation map given in Fig. 6 can be evaluated at every possible temperature. Hereby, the maximal charging current for which no degradation effect occurs is used, i.e. the value in the degradation map at this point is still zero. By evaluating the degradation map over the relevant temperature range, the maximum non-harming charging current as plotted in Fig. 7 can be obtained.

The application of this result for charging control as well as an advanced charging control based on the reduced anode potential model are described in the following Section 4.

4. Charging control

A charging control for lithium-ion cells has to fulfill several requirements and pursues different goals. First of all, the charging control has to guarantee an operation of the battery cells within designated voltage and current limits. Furthermore, it optimizes the charging process, e.g. with respect to charging duration, power dissipation, or degradation effects. Especially at low temperatures, metallic lithium deposition (lithium plating) is a key factor for

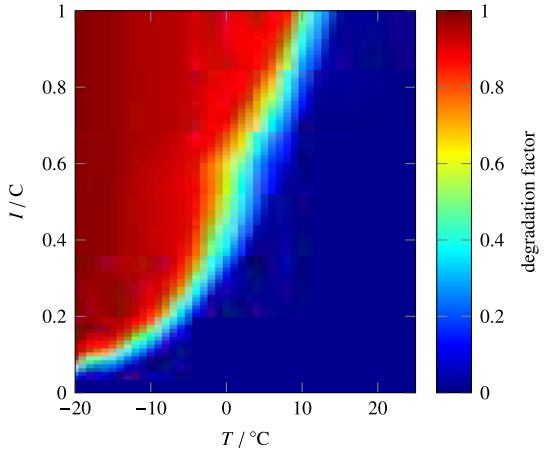

Fig. 6. Degradation map calculated with reduced model.

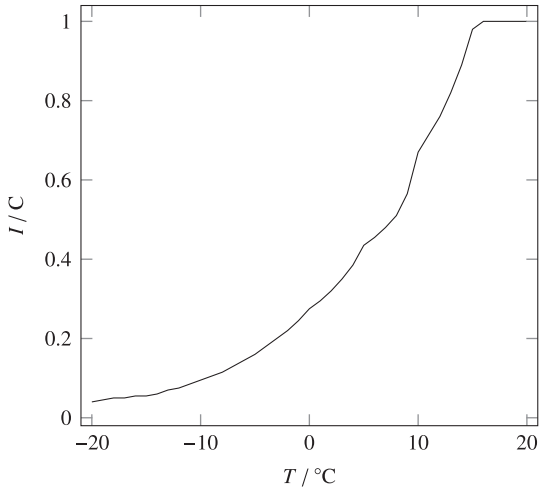

Fig. 7. Maximum non-harming charging current over cell temperature.

degradation. Therefore, in this section, a charging control preventing degradation due to lithium deposition is worked out. As described in Part I [2], extensive laboratory measurements have been carried out to identify the non-harming charging conditions and to model these in a complex electrochemical model. The presented strategy is the result of this measurement study in combination with a complex influence analysis. To be real-time capable, it uses the reduced anode potential model.

The electrochemical model allows a deeper insight into internal cell characteristics especially for charging at low temperature scenarios and therefore offers the possibility to determine a maximum current not leading to degradation. Consequentially, the first approach is to charge the battery cell with a temperature dependent maximum current. These current values are only depending on temperature and can be used independently of the SOC. Such a maximum current can be determined from a degradation map as described in Section 3.2 by repeated simulations of the reduced model quite fast. The determined maximum current depending on current temperature as given in Fig. 7 can be stored in a static table and used easily in a BMS.

With this approach, a full charge divides into two phases. A constant current (CC) phase, during which the battery cell is charged with a maximum current only depending on cell temperature as determined offline with the reduced models, is followed by a constant voltage (CV) phase after the end-of-charging voltage is reached and the current is reduced by a controller to keep the terminal voltage at this value. The charging ends if a predefined minimum current is reached. If heating of the cell occurs, e.g. self-heating due to power dissipation, the charging current is adapted according to the static pre-calculated curve. This controller approach is called CC/CV in the following.

A second, more sophisticated approach directly uses the reduced anode potential model in the BMS. If the anode potential is used as an indicator for degradation during charging, it is sufficient to control the cell current in a way that the anode potential never drops below 0 V. However, the anode potential is a non-measurable value during operation. Therefore, a model of the battery cell which is online applicable on-board a BMS can deliver this additional, non-measurable information.

The anode potential model gained by the model reduction process considers all computational and real-time requirements specified in Section 1. Therefore, it is applicable within a BMS. It requires a reliable SOC value of the cell and is evaluated with a constant sample time for the measured cell current and temperature. Then, the anode potential calculated with the model can be used in an advanced charging control. To account for the small approximation errors of the reduced model, an additional safety margin of 0.01 V has been used for the anode potential for the following investigations.

A block diagram of a possible setup of such a controller is given in Fig. 8, where the reduced model runs in parallel to the measurement of the battery cell. The charging controller determines the optimal charging current from the measured terminal voltage and the simulated anode potential. To keep the additional effort for the controller as low as possible, a minimum block is inserted here ahead of the controller. It determines the minimum of the simulated anode potential and the control deviation of the terminal voltage to the end-of-charging voltage, allowing to use only one controller for both signals. This is possible as both values need to be kept above 0 V and the value closer to zero is sufficient to determine the maximum current. Then, the controller itself can be a common PI controller. In this approach, the maximum charging current I_{max} is no longer statically determined with respect to temperature, but only depending on the available charging power.

For this charging control setup, a full charge is now divided into three phases. These phases are illustrated in Fig. 9. The first phase is a CC phase as already described for the CC/CV approach, where the terminal voltage stays below the end-of-charging voltage and the anode potential is above 0 V. In this phase, the current is only limited by the charger. The lower the temperature, the shorter is this first phase. If the anode potential drops to 0 V, the second phase starts and the controller limits the current to keep the value of the anode potential short above 0 V. This is an additional phase in comparison to the common CC/CV approach described above and is called constant anode potential phase (CP) here. As the charging continues, the terminal voltage will reach its end-of-charging value and the CV phase starts, where the controller further reduces the current as the control deviation of the terminal voltage to the end-of-charging voltage is now passed

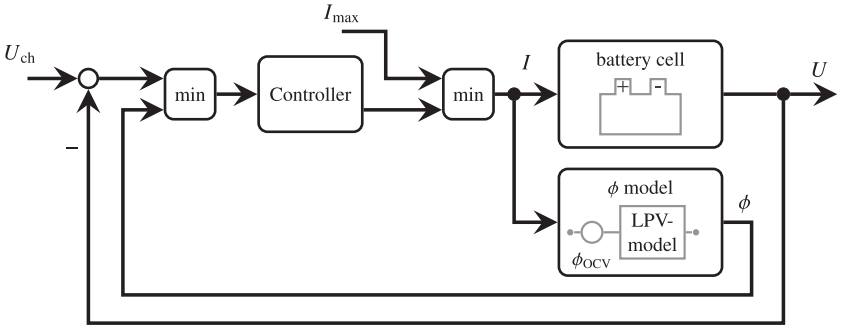

Fig. 8. Advanced charging control.

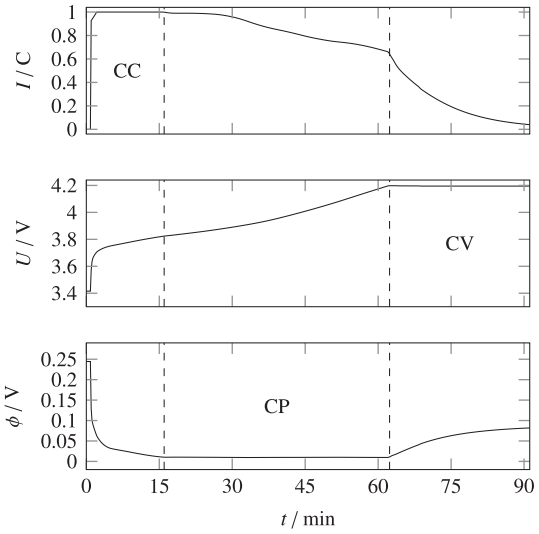

Fig. 9. Illustration of advanced charging control.

through the minimum block. In this CV phase, the anode potential usually rises again. Charging still ends if a predefined minimum current is reached in the CV phase. This controller approach is referred to as CC/CP/CV in the following.

To compare these two charging controller approaches in simulation, the reduced cell model presented in this contribution was coupled with a common heating model. The heating model describes self-heating of the cell due to power dissipation. With this model, the presented controllers were implemented in SIMULINK and tested in different scenarios.

An example of such a comparison of the controllers is given in Fig. 10. The current and cell temperature signals are displayed for the CC/CV controller in orange and for the CC/CV/CP controller in blue. For both controllers, charging begins at identical initial conditions, i.e. an SOC of 0% and a constant ambient and initial cell temperature of −10 °C. The CC/CV controller remains in the CC phase for a great part of the overall charging duration with an almost constant current only slowly rising due to self-heating of the cell. The CC/CV/CP allows a much higher current at the begin of the charging process, until the anode potential drops to 0 V. Then, the charging current is also reduced. It can be seen that the CC/CV/CP controller especially involves the actual SOC during charging and the history of the charging process. Due to these facts, the CC/CV/CP controller achieves a significant reduction of charging duration. Furthermore, due to higher charging currents, increased self-heating occurs which allows for even higher charging currents

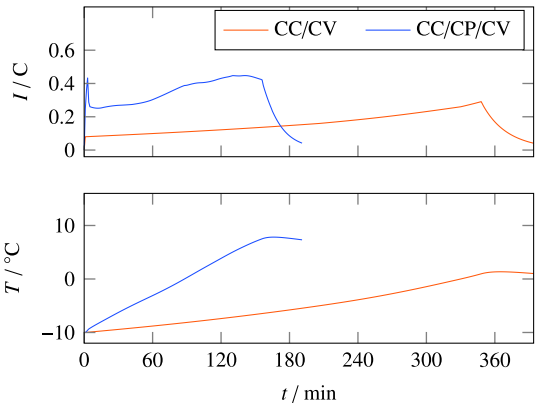

Fig. 10. Comparison of charging strategies regarding duration and temperature.

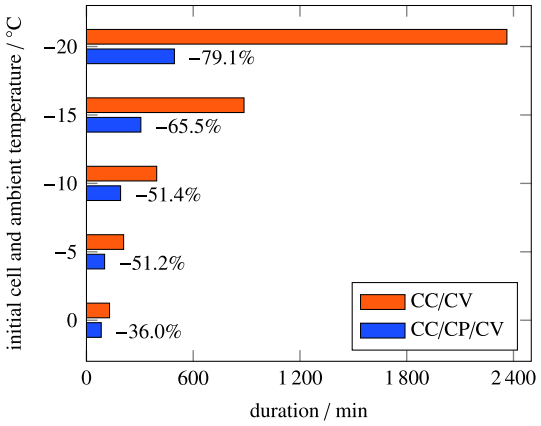

Fig. 11. Comparison of charging durations.

and a faster charging, which results in a positive feedback loop. The final charging time reduction is therefore a combination of higher charging currents due anode potential adaptive current limits as well as the effects of the consequentially resulting positive feedback loop for self-heating. Finally, with this controller strategy, the charge process ends at a higher cell temperature, which is advantageous for a usage of the vehicle soon after the end of the charging process. This higher final cell temperature also leads to the effect that the stored amount of charge is slightly higher for the CC/CP/CV controller in all investigated cases.

To get an overview on possible reductions of charging times, several simulations have been carried out to compare the CC/CV/CP controller with the simpler CC/CV controller. All simulations start with an SOC of 0%, but at different initial cell and ambient temperatures. The resulting charging durations of both controllers for a full charge are shown in Fig. 11. The possible reduction of charging duration varies in the range of nearly 80% at −20 °C and still over one third at 0 °C.

For validation purposes, the both described charging methods have been compared in laboratory for two single cells of the same type. Both cells were cycled at an ambient temperature of 0 °C with the same discharge procedure and either the CC/CV or the CC/CP/CV charge profile for several cycles. To prove that the higher currents for the latter charging method do not lead to degradation, both cells were characterized in a standard test to determine their cell capacity before and after the cycling. Thereby, a reduction of charging duration for the cell charged with the CC/CP/CV controller and no additional degradation compared to the cell charged with the CC/CV controller could be observed, as expected from the simulations. Although these tests cannot be directly compared to the simulation results in numbers because the thermal behavior of a single cell in a test chamber varies significantly from the simulation scenario in a battery pack, it still is a qualitative validation of the proposed method.

5. Conclusions

In this second part of the contribution, an identification-based model-reduction process for terminal voltage and anode potential models from an electrochemical lithium-ion battery cell model was developed. Identification was performed for temperature local LTI models using subspace identification, and these models where combined in one reduced overall model in LPV form for each of the two output signals. The validation of both models on additional simulations of the electrochemical reference model showed a high accuracy. The reduced models have a discrete-time form allowing for fast computation and on-board application, which

was shown in an analysis of the achievable reduction of computation time.

Furthermore, the reduced anode potential model was used to developed an advanced charging strategy. The information obtained by online simulation of the reduced anode potential model is used to control the current such that the anode potential never drops below 0 V in a so-called constant potential phase, and therefore to prevent degradation during charging by lithium plating. This charging strategy was shown to lead to a significant reduction of charging duration at low temperatures in several simulations and a first laboratory measurement.

Future work will focus on further validation of the charging control for single cells in experiment and the application of the anode potential model and charging strategy on-board an electric vehicle.

References

[1] J. Zhang, J. Lee, J. Power Sources 196 (2011) 6007–6014.
[2] S. Tippmann, D. Walper, L. Balboa, B. Spier, W.G. Bessler, J. Power Sources 252 (2014) 305–316.
[3] T.F. Fuller, M. Doyle, J. Newman, J. Electrochem. Soc. 141 (1) (1994) 1–10.
[4] M. Doyle, J. Newman, A.S. Gozdz, C.N. Schmutz, J.-M. Tarascon, J. Electrochem. Soc. 143 (6) (1996) 1890–1903.
[5] J. Remmlinger, M. Buchholz, T. Soczka-Guth, K. Dietmayer, J. Power Sources 239 (2013) 689–695.
[6] R.D. Perkins, A.V. Randall, X. Zhang, G.L. Plett, J. Power Sources 209 (2012) 318–325.
[7] M. Guo, G. Sikha, R.E. White, J. Electrochem. Soc. 158 (2) (2011) A122–A132.
[8] K. Smith, C. Rahn, C.-Y. Wang, in: IEEE International Conference on Control Applications (2008), 2008, pp. 714–719.
[9] N. Chaturvedi, R. Klein, J. Christensen, J. Ahmed, A. Kojic, IEEE Control Syst. 30 (3) (2010) 49–68.
[10] L. Ljung, System Identification: Theory for the User, second ed., Prentice Hall, Upper Saddle River, 1999.
[11] A.M. Colclasure, B.M. Sanandaji, T.L. Vincent, R.J. Kee, J. Power Sources 196 (1) (2011) 196–207.
[12] B.M. Sanandaji, T.L. Vincent, A.M. Colclasure, R.J. Kee, J. Power Sources 196 (2011) 208–217.
[13] G.L. Plett, J. Power Sources 134 (2004) 262–276.
[14] J. Remmlinger, M. Buchholz, M. Meiler, P. Bernreuter, K. Dietmayer, J. Power Sources 196 (2011) 5325–5331.
[15] W.E. Larimore, in: Proceedings of the American Control Conference, San Francisco, 1983, pp. 175–181.
[16] W.E. Larimore, in: Proceedings of the American Control Conference, San Diego, 1999, pp. 1148–1162.
[17] P. van Overschee, B. de Moor, in: Proceedings of the IFAC World Congress, vol. 7, 1993, pp. 361–364. Sydney.
[18] P. van Overschee, B. de Moor, Subspace Identification for Linear Systems: Theory — Implementation — Applications, Kluwer Academic, Boston, 1996.
[19] M. Verhaegen, P. Dewilde, Int. J. Control 56 (5) (1992) 1187–1210.
[20] M. Verhaegen, V. Verdult, Filtering and System Identification – A Least Squares Approach, Cambridge University Press, Cambridge, 2007.
[21] A. Chiuso, G. Picci, Automatica 41 (3) (2005) 377–391.
[22] A. Chiuso, IEEE Trans. Autom. Control 52 (10) (2007) 1795–1812.
[23] M. Buchholz, Subspace-Identification zur Modellierung von PEM-Brennstoffzellen-Stacks, in: Schriften des Instituts für Regelungs- und Steuerungssysteme, vol. 7, Karlsruher Institut fr Technologie, KIT Scientific Publishing, Karlsruhe, 2010.
[24] D. Bauer, Some Asymptotic Theory for the Estimation of Linear Systems Using Maximum Likelihood Methods or Subspace Algorithms (Ph.D. thesis), Technische Universitt Wien, 1998.
[25] T. Katayama, Subspace Methods for System Identification, Springer, London, 2005.
[26] S.J. Qin, Comput. Chem. Eng. 30 (10–12) (2006) 1502–1513.
[27] I. Houtzager, J.-W. van Wingerden, M. Verhaegen, Predictor-based Subspace Identification Toolbox, Version 0.4, 2010 last visit in September 2011, URL: http://www.dcsc.tudelft.nl/~datadriven/pbsid/.
[28] C. De Boor, A Practical Guide to Splines, Springer, 1978.
[29] I. Bronshtein, K. Semendyayev, G. Musiol, H. Mühlig, Handbook of Mathematics, Springer-Verlag, Berlin Heidelberg, 2007.
[30] J.W. Brewer, IEEE Trans. Circuit Syst. 25 (9) (1978) 772–781.
[31] T. Kailath, Linear Systems, in: Prentice-Hall Information and System Sciences Series, Prentice-Hall, 1980.
[32] J.-W. van Wingerden, Control of Wind Turbines with 'Smart' Rotors: Proof of Concept & LPV Subspace Identification (Ph.D. thesis), Technische Universiteit Delft, 2008.